ACS Sustainable Chemistry & Engineering

pubs.acs.org/journal/ascecg

Research Article

Long-Term Hindrance Effects of Algal Biomatter on the Hydration Reactions of Ordinary Portland Cement

Meng-Yen Lin, Paul Grandgeorge, Andrew M. Jimenez, Bichlien H. Nguyen, and Eleftheria Roumeli*

Cite This: *ACS Sustainable Chem. Eng.* 2023, 11, 8242−8254

Read Online

ACCESS | Metrics & More | Article Recommendations | Supporting Information

ABSTRACT: The incorporation of carbon-fixing materials such as photosynthetic algae in concrete formulations offers a promising strategy toward mitigating the concerningly high carbon footprint of cement. Prior literature suggests that the introduction of up to 0.5 wt % chlorella biological matter (biomatter) in ordinary Portland cement induces a retardation of the composite cement's strength evolution while enabling a long-term compressive strength comparable to pure cement at a lower carbon footprint. In this work, we provide insights into the fundamental mechanisms governing this retardation effect and reveal a concentration threshold above which the presence of biomatter completely hinders the hydration reactions. We incorporate *Chlorella* or *Spirulina*, two algal species with different morphology and composition, in ordinary Portland cement at concentrations ranging between 0.5 and 15 wt % and study the evolution of mechanical properties of the resulting biocomposites over a period of 91 days. The compressive strength in both sets of biocomposites exhibits a concentration-dependent long-term drastic reduction, which plateaus at 5 wt % biomatter content. At and above 5 wt %, all biocomposites show a strength reduction of more than 80% after 91 days of curing compared to pure cement, indicating a permanent hindrance effect on hardening. Characterization of the hydration kinetics and the cured materials shows that both algal biomatters hinder the hydration reactions of calcium silicates, preventing the formation of calcium hydroxide and calcium silicate hydrate, while the secondary reactions of tricalcium aluminate that form ettringite are not affected. We propose that the alkaline conditions during cement hydration lead to the formation of charged glucose-based carbohydrates, which subsequently create a hydrogen bonding network that ultimately encapsulates calcium silicates. This encapsulation prevents the formation of primary hydrate products and thus blocks the hardening of cement. Furthermore, we observe new hydration products with composition and micromorphology deviating from the expected hardened cement compounds. Our analysis provides fundamental insights into the mechanisms that govern the introduction of two carbon-negative algal species as fillers in cement, which are crucial for enabling strategies to overcome the detrimental effects that those fillers have on the mechanical properties of cement.

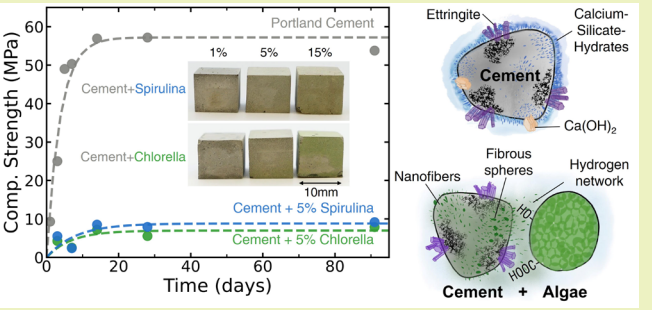

KEYWORDS: *cement, Chlorella, Spirulina, hydration reactions, retardation, sustainability, carbon sequestration*

INTRODUCTION

Accounting for between 5% and 11% of the global emissions of CO_2, the cement industry is one of the primary sources of carbon emission in the world.[1,2] Among the greenhouse gases emission, 50% is attributed to the calcination process which converts limestone ($CaCO_3$) to calcium oxide (CaO), 40% to the fossil fuel combustion during cement manufacturing, and 10% to transportation and operation activities.[3] Substantial research has been conducted to address this harmful environmental impact over the past three decades, including predicting the strength of hydrated cements through molecular dynamics simulations[4−7] which enables the use of less cement material in applications without sacrificing performance, improving the energy efficiency of the manufacturing process,[8] carbon sequestration through carbonation curing,[9] and reducing clinker/cement ratio by introducing additives such as fly ash (industrial waste),[10] glass (municipal waste),[11] and rice husk ash (natural waste from agricultural and aquacultural farming).[12]

Renewable and carbon-sequestering biological materials provide alternative additives to improve the environmental footprint of cement while enabling additional functionalities. For example, certain bacteria, mycelia, and enzymes have been used to induce biomineralization in self-healing concrete,[13−17] and plant-derived cellulose has been introduced in cement as

Received: December 21, 2022
Revised: May 9, 2023
Published: May 23, 2023

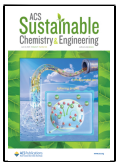

macro- and nanoscale reinforcement.[18−22] Cellulose, in particular, is used as an internal curing agent and water transport pathway to improve cement's access to water, thereby increasing the degree of hydration in cement and further reinforcing mechanical properties. Indeed, in a review by Guo et al.,[21] the authors report that fillers in the form of cellulose nanocrystals (CNCs) and cellulose nanofibrils (CNFs) induce a delaying effect on cement hydration but can lead to higher late-age strengths. For example, Fu et al.[23] reported an increase in flexural strength from 22.0 to 28.8 MPa (+30.1%) in Portland cement when filled with 2 vol % (CNC/dry cement) tested at day 28. It should however be noted that cellulose often requires cost and energy intensive processing steps for extraction and functionalization, thereby still limiting its large-scale use.

Another approach, which has been applied widely, consists of using entire plant fibers as reinforcement (e.g., in structural concretes).[24] For example, bamboo fibers were used by Akinyemi et al.[25] at concentrations between 1 and 1.5 wt % (fibers/total mass of constituents) in a cement and sand mortar mix. Comparing three different fiber pretreatment methods (hot water, microwave irradiation assisted alkaline treatment, and alkali treatment only), they showed that the microwave assisted alkaline treatment leads to the highest flexural strength compared to the two other treatments. The authors suggest that the microwave assisted alkaline treatment, through the removal of cellulose, lignin, and hemicellulose from the fiber's molecular structure, leads to a roughening of the surface, which enables the cement hydrates to fill the voids, in turn leading to improved adhesion with the cement matrix. In another study, Ban et al.[26] showed that without fiber treatment or additives, the incorporation of 2 vol % bamboo decreases strength from 51.2 to 37.0 MPa (−27.7%). Other examples of plant fibers and tissues as fillers include sugar cane bagasse,[27] hemp,[9] flax,[28] straw,[29] jute, and kenaf.[24]

As an alternative biological-origin filler, algae and algae-derived materials have been receiving increasing attention as their applications broaden from nutraceuticals and pharmaceuticals to biofuels and bioplastics, owing to their advantageous rapid growth rates and scalable cultivation with low land usage compared to other plants.[30−32] Moreover, the high capacity of carbon sequestration (1 kg of dry algal biomass absorbs roughly 1.8 kg of CO_2[33]) marks a key benefit of utilizing algal materials, especially in high-volume applications, such as construction materials, when attempting to reduce environmental impact. In cement formulations, specifically, algae-derived biopolymers have been long utilized as viscosity modifiers and agents to control volume changes upon hydration. For example, alginate, extracted from the cell walls of brown algae, has been used to controllably change the viscosity of cement pastes[34] or to improve the mechanical properties and durability against chloride penetration of hardened cement.[35] Carrageenan, another algal cell wall biopolymer, has been leveraged as superabsorbent polymer to improve the autogenous shrinkage in cement pastes.[36] A considerable amount of prior work has focused on understanding the effects of plant- or algae-derived biopolymers on cementitious materials, but the production of these renewable biopolymers involves energy-intensive steps such as mechanical disintegration followed by long hydrolysis reactions in acidic[37,38] or alkaline[39] solutions. These processing routes are typically low yield, as only a small fraction of the dry mass is extracted as a product, while the remaining parts of the biomass are manufacturing waste. A recently emerging and more sustainable alternative[40−43] suggests using fast-growing, untreated plant, algal, or microbial biomatter, in the form of intact cells or tissues, as a polymeric matrix or filler material, aiming to capitalize on raw biomatter to function as a renewable material platform that potentially can lead to wasteless processes. Photosynthetic biomatter in particular, such as plant or algal cells, can effectively serve as carbon-negative matrix materials or additives. The concept of utilizing abundant and intact algal biomatter in the design of hybrid cementitious formulations remains, to a great extent, unexplored. Chen et al.[44] recently provided the first insights into the effects of introducing ceased chlorella cells, in the form of ground-up pellets, on the mechanical properties of cement. Their work shows that the incorporation of 0.5−3 wt % chlorella powder aggregates into Type I/II Portland cement effectively delays the cement hydration reactions by 16−800%. Further, they estimate that cement composites containing 0.5 wt % chlorella allow for a 1% reduction in the embodied carbon of cement while not affecting the compressive strength. Yet, the mechanisms governing the interactions between unprocessed algal biomatter and cement and understanding the biomatter effects on each of the hydration reactions and their concentration dependence remain elusive.

In this work, aiming to expand the design space of sustainable algae−cement formulations and explore higher biomatter concentrations, we study two different types of unprocessed algal biomatter, chlorella and spirulina, introduced at concentrations of 0.5−15 wt % in ordinary Portland cement. We specifically choose these two types of algal species as they are both widely available and have different biopolymer constituents, thus enabling us to discern the effects of polymer composition. While the use of unprocessed algae also ensures no other additives are included in the formulation, the comparable particle sizes of both algae to cement particles allows us to consider the resulting composites as binder materials with potential future applications in mortar or concrete. Through comprehensive characterization, we establish the fundamental impacts of the biomatter inclusions in the cement hydration reactions and their kinetics.

In addition to the known retardation effects induced in the presence of biomatter at low concentrations reported by Chen et al.,[44] our study reveals a long-term significant reduction in compressive strength at biomatter concentrations above 5 wt %, which was previously not reported. We present a detailed characterization of the hydration reaction products and offer new insights on the mechanisms leading to this drastic decrease in the hardening of the composite cements.

MATERIALS AND METHODS

Materials. Commercially available Type I/II Portland cement (SAKRETE, Charlotte, NC, USA), abiding by ASTM c150,[45] was used as our cement matrix. The chemical composition of the Portland cement is shown in Table 1. Chlorella and spirulina powders were purchased from Nuts.com (Cranford, NJ, USA). The moisture content of chlorella and spirulina powders was measured in the range

Table 1. Oxide Content (wt %) of Type I/II Portland Cement Used in This Paper

CaO	SiO_2	SO_3	Al_2O_3	MgO	Fe_2O_3	K_2O	Na_2O
67.14	14.00	9.68	3.51	1.70	2.81	0.89	0.28

https://doi.org/10.1021/acssuschemeng.2c07539
ACS Sustainable Chem. Eng. 2023, 11, 8242−8254

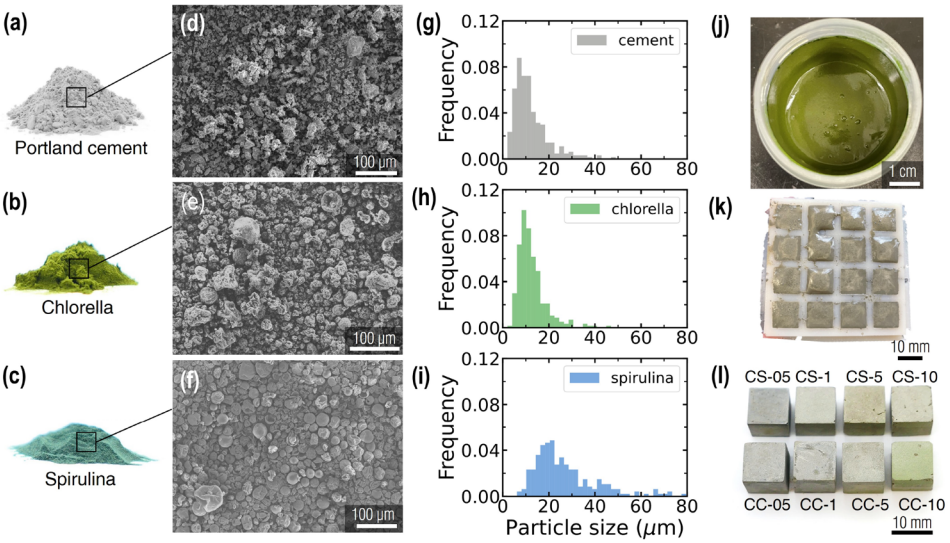

Figure 1. Powder characterization and sample fabrication. (a–c) Photographs of the cement, chlorella, and spirulina powders, respectively. (d–f) Corresponding SEM images of each powder. (g–i) Particle size distribution of the three dried powders. (j) Cement–chlorella–water paste before casting (hereafter, 5 wt % chlorella). (k) Casting of the biocomposite cubes. (l) Photographs of the green cement samples upon demolding.

of 6–8 wt % of the biomatter with a moisture analyzer (VWR-53M.H, VWR, Radnor, PA, USA).

Sample Preparation. Biomatter powder was premixed with cement powder at concentrations of 0.5%, 1%, 5%, 10%, and 15% by weight of total dry mass using a speedmixer (SpeedMixer DAC 330-100 PRO, FlackTek, Landrum, SC, USA) operating at 1500 rpm for 30 s. Next, deionized water was progressively added to the mix to produce pastes which were further homogenized in the same mixer (operating at 1500 rpm for a total of 180 s with three 15 s breaks every 45 s). All the cement pastes were prepared at a fixed water–cement ratio (w/c) of 0.4. Note that, in order to keep only the essential components of this mix and avoid unexpected interactions, no water reducing admixtures were added to the pastes. Then, the mixed fresh pastes were cast into rubber molds to produce cubic samples with nominal dimensions of 10 × 10 × 10 mm^3. The cast slurries were rodded on a vibration table (No.1A vibrator, Buffalo Dental Manufacturing Co. Inc., Syosset, NY, USA) to eliminate macroscopic air bubbles. After casting, the fresh samples were sealed with plastic films and placed in a moisture-controlled chamber to cure at 90 ± 5% RH and 23 ± 1 °C for 24 h before demolding. A pure cement (PC) sample at w/c 0.4 was made with the same procedure as a reference in comparison to the cement–chlorella composites (CCs) and cement–spirulina composites (CSs) at varying algal concentrations. Throughout this Article, samples are labeled to reflect their components and concentrations. For example, CS-0.5 corresponds to the cement–spirulina composition at 0.5 wt % spirulina and CC-5, to cement–chlorella at 5 wt % chlorella.

Compression Tests. Compression testing (Figure S1a) was performed on a minimum of 5 samples for each mixture after 3, 7, 14, 28, or 91 days of curing using a universal test frame (Autograph AGS-X 10kN, Shimadzu Scientific Instruments, Columbia, MD, USA) equipped with a 5 kN load cell. The cubic samples were compressed at a constant stress rate in accordance with ASTM C109/C109 M.[46] The stress, σ, was calculated from $\sigma = F/A$, where F is the measured force and A is the cross-sectional area. The compressive strain was calculated as $\epsilon = d/H$, where d is displacement and H is the initial sample height. Maximum compressive strength is obtained from the stress–strain curve, as the maximum stress value withstood by the samples prior to fracture.

Scanning Electron Microscopy (SEM) and Energy-Dispersive X-ray Spectroscopy (EDS). Samples were coated with 4 nm of platinum in a sputter coater (SC7620, Quorum Technologies, Lewes, U.K.) and imaged with SEM (JSM-6010 Plus, JEOL, Peabody, MA, USA) at an accelerating voltage of 10 kV. Samples for EDS were coated with 4 nm of gold in a sputter coater (108 Manual, Ted Pella, Redding, CA) and detected with SEM (Phenom ProX Desktop SEM, Thermo Fisher Scientific, Waltham, MA, USA) at an accelerating voltage of 10 kV. For the powders, particle size analysis from the acquired images was conducted using ImageJ.[47]

Isothermal Calorimetry (IC). The early stage hydration kinetics were monitored in an isothermal calorimeter (TAM air; TA Instruments, New Castle, DE, USA). Using the 20 mL admix ampules, the heat generated by the hydration reactions was measured at a constant temperature of 24 °C starting from the instant of water–cement contact through the mixing and hardening process until day 7. Quantities related to heat were normalized by the mass of solid powders (cement and biomatter).

Thermogravimetric Analysis (TGA). Samples of 5–8 mg were heated in platinum crucibles from ambient temperature to 1000 °C in a TGA instrument (D550, TA Instruments, New Castle, DE, USA) under a 20 mL/min flow of nitrogen gas. The temperature was first increased to 140 °C at a heating rate of 10 °C/min and was kept constant for 30 min to evaporate the absorbed water in samples and was subsequently increased to 1000 °C at a rate of 10 °C/min.

X-ray Diffraction (XRD). The X-ray diffraction measurement was conducted using a D8 Advance XRD, Bruker, Billerica, MA, USA with Cu Kα X-ray radiation (wavelength 1.5406 Å). The diffraction patterns were measured in the range 5°–70° 2θ with a step size of 0.02° and a collection of 0.07 s/step. The XRD analysis was done using the MDI-500 library (JADE 8.3, Materials Data, Livermore, CA).

Fourier Transform Infrared Spectroscopy (FTIR). Samples were analyzed in an FTIR spectrometer (Nicolet is10 FT-IR; Thermo Fisher Scientific, Waltham, MA, USA) in attenuated total reflection (ATR) mode. The scanning region was set in the range of 7800–350 cm^{-1} with a resolution of 2 cm^{-1} over 64 runs.

RESULTS AND DISCUSSION

In Figure 1, we present the morphological features of the raw chlorella and spirulina cells as well as cement, along with the sample fabrication process. SEM images reveal that the cement particles have a size distribution of 5–20 μm (see Figure 1d,g) with a mean particle size of 13 μm. *Chlorella*, being a unicellular algae, grows in individual cells which obtain a circular shape and do not form tissues. The dehydrated *Chlorella* cells can form aggregates with sizes ranging between

https://doi.org/10.1021/acssuschemeng.2c07539
ACS Sustainable Chem. Eng. 2023, 11, 8242–8254

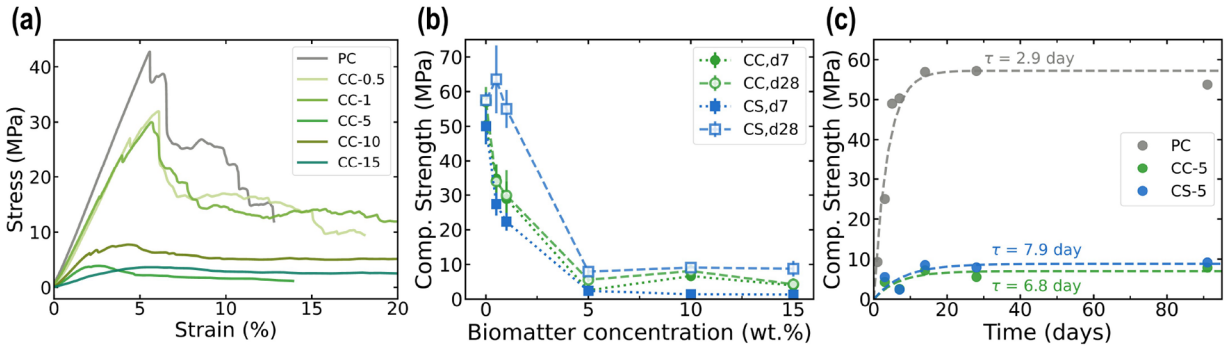

Figure 2. Compressive strength and aging effect of cement composites with chlorella and spirulina. (a) Representative stress−strain curves of cement−chlorella composites tested at day 7. (b) Effect of different concentrations of chlorella and spirulina on the compressive strength of cement composites tested at day 7 and 28. (c) Effect of curing duration on the compressive strength of cement−chlorella and cement−spirulina composites containing 5 wt % biomatter.

10 and 20 μm (Figure 1e,h), while when in the hydrated state, the average particle size of individual cells is 3.7 ± 0.9 μm. *Spirulina* cells, on the other hand, form chains with length of 6−30 μm and width of 6.8 ± 0.8 μm in the hydrated state, which give rise to aggregates of 20−40 μm in the dried state (Figure 1f,i). As presented in Figure 1j−l, the samples containing the target amount of biomatter were mixed into pastes with cement and water, which were subsequently molded into cubic shapes for further analysis.

Effects of Biomatter on Compressive Strength. We assess the effects of each type of biomatter on the mechanical properties of cement through quasi-static compression tests at different ages, as shown in Figure 2. The stress−strain curves of hardened Portland cement and cement−chlorella composites with different concentrations of chlorella (Figure 2a) show an initial linear stress increase, followed by a quasi-brittle fracture as cracks develop in the samples. The same behavior is also found in the spirulina composites (Figure S1b). As anticipated, the incorporation of the soft algal biomatter results in reductions of both the compressive strength and Young's modulus of the composites, which are found to decrease with increasing filler content.

In Figure 2b, we compare the maximum compressive strength of our composites at varying concentrations of biomatter (spirulina and chlorella), tested at day 7 and 28. For both sets of composites, the compressive strength first rapidly decreases with increasing algae concentration, before reaching a low-strength plateau at around 5 wt %. The introduction of 0.5 wt % of either chlorella or spirulina leads to reductions of 7-day compressive strength by 31% and 46%, respectively, compared to pure cement. Upon further increasing the biomatter content to 1 wt %, the 7-day strength of the composites slightly decreases from 34.7 to 28.9 MPa for chlorella and from 27.4 to 22 MPa for spirulina. Increasing the content of algal biomatter to 5 wt % drastically decreases the 7-day compressive strength of both cement−chlorella and cement−spirulina composites to around 2.5 MPa (corresponding to a 95% reduction compared to pure cement), suggesting a clear decay of early strength with increasing concentration.

Although the effects of adding chlorella and spirulina are identical at early ages, the two composites show different performances after longer curing times. At low concentrations, the compressive strength of the spirulina composites increases over time, while the chlorella composites show no strength growth. The 28-day strength of 0.5 and 1 wt % spirulina composites increases to more than 55 MPa (more than 2-fold increase compared to 7-day strength), reaching the same values as pure cement. Similarly, at higher concentrations, the compressive strength values of composites with 5−15 wt % spirulina increase about 3-fold (from 2 to ∼8 MPa) from day 7 to day 28. This result indicates differences in the nucleation and growth-rate kinetics and aging mechanisms at low amounts of chlorella and spirulina, which are more pronounced at later ages. The effects of functional groups and biopolymer composition on the difference of strength evolution between chlorella and spirulina composites is a topic for future investigation.

Still, in both types of microalgae, the drastic reduction of compressive strength with increasing concentration suggests different hydration reactions between composites containing low (0.5−1 wt %) and high (>5 wt %) concentrations of algal biomatter. To further investigate the mechanisms causing such a significant change in the mechanical performance of our composites, the following part of our study focuses on analyzing the structure and properties of composites containing 5 wt % of either chlorella or spirulina, as this concentration was the identified behavioral threshold in both systems.

To monitor the strength evolution over time, chlorella and spirulina composites at 5 wt % biomatter concentration were, respectively, tested in compression on day 3, 7, 14, 28, and 91. In Figure 2c, we present the strength evolution of pure cement and the two sets of composites. The strength of the composites increases most prominently from day 3 to 14, varying from 2.5 to 7.2 MPa for chlorella composites and from 2.4 to 8.4 MPa for spirulina composites. These strength values then remained approximately constant until day 91.

Compared to pure cement samples, whose strength increases from 50% of full strength on day 3 (25 MPa) to 86% on day 7 (50.3 MPa), not only the final strength of the composites is notably lower but also the strength evolution is slower as it increases from 30% of full strength to 90% from day 7 to 14. We propose the use of an exponential expression to quantitatively assess the characteristic evolution time for the compressive strength of our composites:

$$\sigma(t) = \sigma_f(1 - e^{-t/\tau}) \quad (1)$$

In eq 1, σ_f (MPa) corresponds to the final (plateau) strength and τ (days) is the characteristic evolution time, representing the required time of strength to reach a plateau. The fitting

https://doi.org/10.1021/acssuschemeng.2c07539
ACS Sustainable Chem. Eng. 2023, 11, 8242−8254

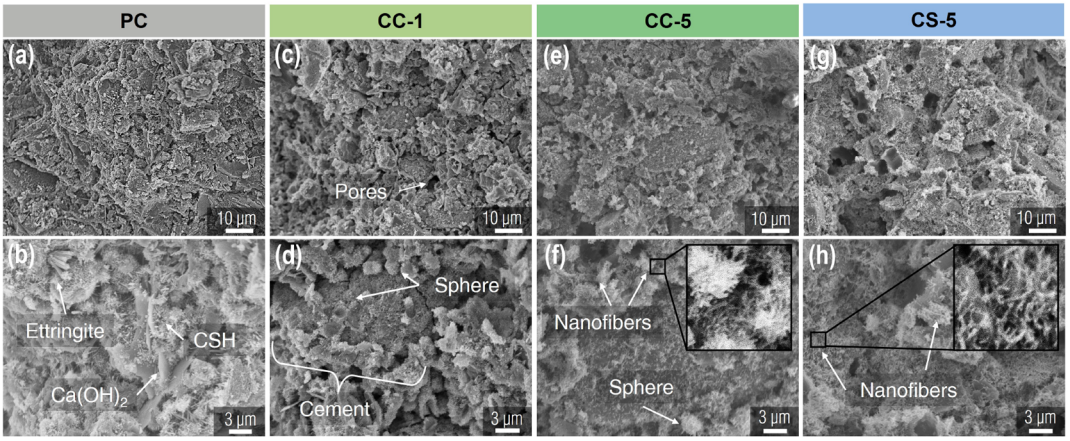

Figure 3. Effects of pure biomatter on the micromorphology of biocomposites. (a, b) SEM images of PC on day 7. (c, d) SEM images of CC-1 on day 7. (e, f) SEM images of CC-5 on day 7. (g, h) SEM images of CS-5 on day 7. The insets in (f) and (h) show the nanofibers at higher magnification.

parameters (σ_f and τ) were computed using the least-square method, and the corresponding curves are presented as dashed lines in Figure 2c. By means of comparison, a τ value of 3.8 days was found for the pure cement versus 6.8 days for the chlorella composites and 7.9 days for the spirulina composites. While the difference in τ shows a delay in strength evolution for the composites, the large difference in final strength, σ_f, between either composites and the pure cement suggests fundamentally different cement−microalgae interactions than the pure retardation effect previously reported in the literature.[44] We note that, in our study, we use unprocessed algae cells of defined particle size and native composition (discussed in detail in the following sections), while in prior literature[44] the chlorella filler was previously pressed in pellets (may or may not contain additives) and then mechanically ground into powder; both processing steps might lead to altered composition and substantially reduced surface area compared to the raw algal biomatter.

Effects of Biomatter on the Micromorphology of Hardened Cement. To investigate the distribution of algal biomatter filler in the cement matrix and the biomatter−cement interactions, we analyze the optical microscopy and SEM images of the biocomposite microstructures on day 7 and 28.

Based on macroscopic and optical microscopy images (reported in Figure S2a,b), we visually observed an increasing size and number of voids (size range tens of μm) at the surfaces of samples with increasing concentrations of algal biomatters. While such micropores may act as structural defects leading to a mechanical embrittlement, the strength of cements is generally tightly dictated by the density and interconnection of hydration products,[4] which we will investigate next.

From SEM images, we observe that the microstructure of pure cement becomes highly dense by day 7 with the anticipated continuous growth of hydration products (Figure 3a,b), as corroborated by its strength value of 86% of the final strength which indicates the nearly plateaued hydration reactions. The micrographs reveal that the calcium hydroxide ($Ca(OH)_2$, also called portlandite) platelets as well as ettringite ($Ca_6Al_2(SO_4)_3(OH)_{12}\cdot 26H_2O$) prisms are well dispersed within the hydrated matrix. The length of ettringite prisms is 0.8−1.7 μm, in agreement with observations that ettringite grows to lengths 1−5 μm at low water-to-cement ratios ($w/c < 0.5$).[48,49] The nanoscale tapered fibers covering the cement particles' surface are amorphous calcium silicate hydrate ($C-S-H$) with lengths 200−400 nm, which can be attributed to the fibrous Type-1 $C-S-H$ described by Jennings et al.[50]

Upon the introduction of algal biomatter, even at only 1 wt % chlorella, fewer $Ca(OH)_2$ platelets and ettringite prisms are found in the composites (Figure 3c,d), and they are almost eliminated at the 5 wt % filler content (Figure 3e,f). The higher magnification views reveal nanofibers with a consistent length of ∼500 nm, covering the composite matrix surface. These nanofibers grow radially outward from the smooth inner cement particle surface. Even though the size of the discovered nanofibers is close to the amorphous $C-S-H$ fibrils found in pure hardened cement, their distribution is significantly different, resulting in a different morphology than pure cement, which suggests that the nanofibers seen in the composites may not be composed of $C-S-H$. Moreover, in the chlorella 1 wt % composites besides the nanofibers, we also observe the formation of distinct interconnected microspheres, 3−5 μm in diameter, matching the average cell size. The similarity in shape and size between these microspheres and the chlorella cells suggest that chemical interactions between the biomatter surface and the cement colloid may occur, which lead to the formation of the observed shells of nanofibers covering the biomatter and anhydrated cement particles and nanofiber clusters, which are observed between anhydrated cement. Finally, both the 1 and 5 wt % chlorella composites have a notably higher porosity than pure cement, which supports their reduced strength. In contrast, the $C-S-H$ nanofibers in pure cement form a dense coating surrounding the cement particles, which they are grown from, and bridge the gaps between the unreacted particles and other reaction products ($Ca(OH)_2$ and ettringite), ultimately generating a dense interconnected matrix.

The SEM images (Figure 3g,h) also reveal that the spirulina composite surfaces are coated by clearly more nanofibers when compared to the chlorella composite surfaces, which supports the 43% higher compressive strength of the 5 wt % spirulina composites compared to the chlorella. In addition, we note that macroscopic pores of 10 to 30 μm are more prevalent in the spirulina composites while smaller pores between 2 and 10

https://doi.org/10.1021/acssuschemeng.2c07539
ACS Sustainable Chem. Eng. 2023, 11, 8242−8254

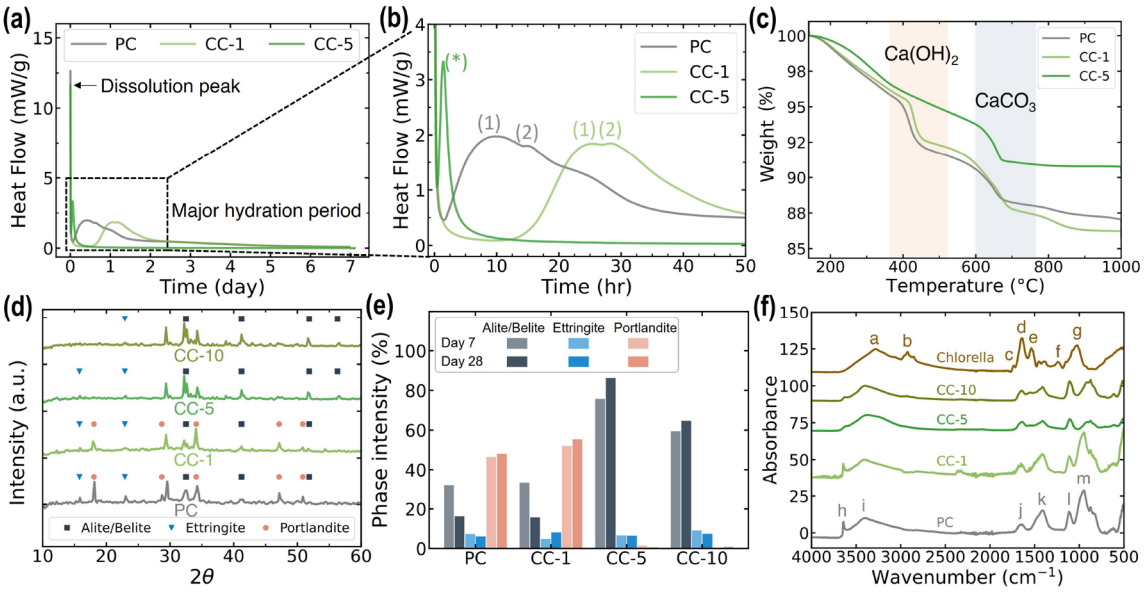

Figure 4. Effects of biomatter on the hydration reactions. (a) Isothermal calorimetry heat flow profile of pure cement and composites with 1 and 5 wt % chlorella in 7 days and (b) zoom-in of the major hydration period. (c) TGA curves of PC, CC-1, and CC-5 on day 28. (d) XRD patterns of CC composites on day 28. (e) Phase evolution of alite or belite, ettringite, and portlandite in CC composites at concentrations of 0.5−10 wt % on day 7 and 28. (f) FTIR spectra of CC composites at concentration of 0.5−10 wt % on day 28.

μm are noted in the chlorella composites. This finding aligns with the larger cavities (10−50 μm) on the surface of spirulina composites in Figure S2g,h, while larger numbers of smaller pores are found in the composites with higher biomatter concentrations (Figure S3a,b). These larger pores in spirulina composites are consistent with the larger size of the spirulina aggregates reported from the particle size analysis of the dry powders (see Figure 1c), highlighting the connection between the formed pores and the cell size.

We expect that, as algal cells dehydrate, losing the bound water over time, the difference between the hydrated versus dried volume of the cells should be reflected in the shrinkage and apparent density of the samples. To quantify these changes, we characterized the overall shrinkage and apparent density of the composite cements over time. We first find that the addition of chlorella and spirulina at low concentrations reduces the shrinkage of samples (see Supplementary text and Figure S3c,d). At day 28, PC samples had shrunk by 0.3%, whereas CC-1 and CS-1, respectively, shrunk by 0.2% and 0.25%, suggesting the biomass slowly releases water over time and stabilizes the bulk volume. Such a slow water release might have a beneficial internal curing effect, enabling a prolonged period of water accessible to the hydrating cement particles and thereby leading to higher final strengths. However, our strength measurements did not suggest strength improvement, implying that internal curing does not take place in our composites. At higher filler concentrations, samples were too weak to allow precise shrinkage measured over time. Apparent density measurements were used to assess water evaporation of the composites. Indeed, the decreasing apparent density with increasing biomatter concentrations (Figure S3e) not only account for the lower density of algal biomatter (1.3 g/cm^3) but also suggest a facilitation of water evaporation at high biomatter concentrations (for calculations of evaporated water, see the discussion in the SI). For example, when more than 5 wt % algae is introduced, the apparent density of biocomposites at day 28 is as low as the theoretical density prediction from eq 5 in the SI, when assuming 100% water evaporation. This drastic water evaporation over time suggests that, in those biocomposites, water only marginally participates to the hydration process, leading to the weak mechanical properties and distinct porous microstructure aforementioned. Next, the hydration reaction is studied more in depth.

Effects of Biomatter on the Hydration Reactions. To further investigate the compositions of the nanofibers and potentially altered hydration reactions, we characterized the pure cement and the composites using IC, TGA, XRD, FTIR, and EDS. The heat flow measured by isothermal calorimetery allows one to monitor the hydration kinetics at early age until day 7 (Figure 4a). Focusing on the major hydration periods as shown in Figure 4a, the first extensive heat flow peak within the first hour corresponds to the ion dissolution and activation of tricalcium aluminate hydration reactions. The following induction period (time period before the onset of the primary reaction) of composites containing 1 wt % biomass is prolonged by a factor 6.25 compared to pure cement (from 2 h for pure cement to 12.5 h for the biocomposite), and the dominant hydration peaks during the acceleration period are delayed from 10 h after mixing to 26 h. Meanwhile, the time difference between the first silicate hydration peak (marked as 1 in Figure 4b) and the second aluminate hydration peak with the depletion of sulfate (peak 2) is 1 h shorter with the addition of 1 wt % chlorella. These suggest that, at low concentration, biomatter slows down the nucleation of *C*−*S*−*H* and Ca(OH)$_2$ and promotes the depletion of sulfate. With the addition of 5 wt % chlorella, the heat flow profile is radically modified. With the exception of the same initiation peak in the first hour, the dominant hydration peaks entirely disappear even until day 7 (see Figure 4a) while a new peak with heat flow content of 3.3 mW/g appears at 1.4 h (labeled (*) in Figure 4b; not observed in PC and CC-1), possibly suggesting a distinct chemical reaction between the algal biomatter and the cement colloid.

https://doi.org/10.1021/acssuschemeng.2c07539
ACS Sustainable Chem. Eng. 2023, 11, 8242−8254

Combining the mechanical performance and the calorimetry results, we have thus far shown that introducing low-concentration algal biomatter into ordinary Portland cement causes a retardation effect whereas long-term hindrance is induced at concentrations higher than 5 wt %. Highlighting the altered hydration reactions, we now focus on the hydration products to further assess the interactions between the biomatter fillers and cement.

The mass loss profiles collected through TGA allow quantification of the water, $Ca(OH)_2$, and calcium carbonate $CaCO_3$ contents in our materials. The TGA curves of pure cement, and the chlorella composites with 1 and 5 wt % biomatter samples tested at day 28 are shown in Figure 4c. The initial mass loss from room temperature to 140 °C corresponds to water adsorbed by the samples, including the water contained in the cement pores and uptaken by the biomatter. This water content is reported in Figure S3f for each sample. In combination with the increased porosity observed in Figures 3 and S3e,f as well as the decreased apparent density, the lower pore water content in the composites containing more than 5 wt % algal biomatter confirms that more water evaporation occurs over time at higher algae contents. This water evaporation is likely due to fewer hydration products stabilizing pore water and a loose microstructure (facilitated by the suppressed hydration reactions), which enables more rapid water diffusion toward the surface. To facilitate the thermogravimetric analysis of our hydration products using the chemically bound water, we exclude the effect of pore water by setting the sample mass at 140 °C as 100% for all samples in Figure 4c. For pure cement, the first significant mass loss takes place between 380 and 520 °C and is associated with the decomposition of $Ca(OH)_2$ to CaO ($Ca(OH)_2 \rightarrow CaO + H_2O$), while the second decomposition occurring between 600 and 780 °C is attributed to $CaCO_3$ ($CaCO_3 \rightarrow CaO + CO_2$).[51] The rest of mass loss ranging from 140 to 1000 °C is attributed to the chemically bound water within ettringite or the *C*−*S*−*H* interlaminar structure.[51,52]

The chlorella composite with 1 wt % biomatter shows a degradation profile qualitatively similar to pure cement. From the first mass loss stage, we calculate that the $Ca(OH)_2$ content is 3.5% in pure cement and 3% in the chlorella 1 wt % composite. The second mass loss stage reveals a calcium carbonate content of 3% for pure cement and 3.5% for the composite.

However, the distinct decomposition of $Ca(OH)_2$ in the range of 380−520 °C is not observed for the composite with 5 wt % chlorella, while the calcium carbonate mass loss step is evident and shows a 3% content in that composite. This result implies that the introduction of algal biomatter at a concentration of 5 wt % prevents the primary hydration reactions in ordinary Portland cement where alite (Ca_3O_5Si) and belite (Ca_2O_4Si) react with water to create *C*−*S*−*H* and $Ca(OH)_2$ and therefore eliminate the silicate hydration peak in the calorimetry heat profile.

Comparing the XRD patterns of pure cement and the chlorella composites at different concentrations (Figure 4d), we observe that peaks at 18.1°, 28.7°, 47.1°, and 50.8° are gradually decreased as the biomatter content increases, and at 5 wt %, they are absent from the collected patterns. These peaks correspond to $Ca(OH)_2$,[53−55] and therefore, their absence in the 5 wt % chlorella composite corroborates the TGA findings that indeed this hydration product is either never formed or entirely depleted in the presence of 5 wt % biomatter. On the other hand, the peaks at 32.3°, 32.6°, 41.3°, and 52°, attributed to anhydrated cement silicates (alite and belite),[56−58] are prominent and even found to be increasing with increasing chlorella content, indicating the existence of unhydrated reactants. Although the peaks associated with anhydrated cement were observed even at the composites with 10 wt % chlorella, we note that ettringite peaks (located at 15.8° and 22.9°) appear,[53,55] albeit at low intensity, in the XRD patterns of chlorella composites with up to 5 wt % biomatter. As ettringite is the earlier-formed product of cement hydration, the detection of these peaks suggests that the hydration reactions, where tricalcium aluminate ($Ca_3Al_2O_6$) reacts with gypsum and water, were activated when the mixture was in contact with water.

Phase analysis through peak deconvolution of the XRD patterns of biocomposites is conducted at varying biomass concentrations on both day 7 and 28. The phase evolutions of the anhydrated cement (alite/belite), ettringite, and portlandite in chlorella composites are shown in Figure 4e. The amount of alite and belite reduces over time with a slight increase in portlandite in pure cement and the composites with low biomass additions, which suggests a continuous hydration process in those materials. Throughout the 28-day curing duration, the absence of portlandite in composites containing more than 5 wt % chlorella and the relatively high amount of anhydrated cement (∼60−80%) again confirms the impeded primary hydration reaction caused by the addition of chlorella at high concentration. We note the presence of ettringite remains at ∼6% in all of the biocomposites over time, indicating that the initial formation of ettringite indeed happens while the constant volume suggests lack of extensive monosulfate transformation. Hence, we propose that only the primary hydration reactions of alite and belite are hindered in the presence of chlorella biomatter at high concentration. In the early hydration reaction stage, during which ettringite is formed, our results show that the cement particles have access to water, but the strength acceleration stages that require *C*−*S*−*H* and $Ca(OH)_2$ formation are hindered.

The same conclusions can be drawn for the spirulina composites with the ettringite XRD peaks being present even at 10 wt % biomatter content (Figure S4) and the alite and belite peaks showing increasing intensity with the increase of biomatter content. Interestingly, we detect a new amorphous feature from the broad peak between 15° and 23° in the spirulina patterns (Figure S4a), suggesting the presence of amorphous products, similar to the *C*−*S*−*H* form which results in an amorphous peak between 15° and 25°.[59] In addition, the presence of 10% portlandite in spirulina composites CS-5 and CS-10 (Figure S4b) suggests that introducing spirulina induces less hindrance effect on the primary hydration reaction compared to chlorella. These results support the measured higher compressive strength and capability of strength growth over time of spirulina compared to the chlorella composites. This finding is in agreement with the SEM observation of spirulina composites, which are covered with a denser layer of nanofibers compared to chlorella composites.

Based on our characterizations from SEM, TGA, and XRD, we consistently detect the elimination of $Ca(OH)_2$, the presence of ettringite, and increasing amounts of anhydrated alite and belite. However, we have not yet identified whether the nanofibers detected in the composites are *C*−*S*−*H* or ettringite or whether they are the byproducts of algal biomatter and cement. Since *C*−*S*−*H* and $Ca(OH)_2$ are both formed as

https://doi.org/10.1021/acssuschemeng.2c07539
ACS Sustainable Chem. Eng. 2023, 11, 8242−8254

products of the same hydration reactions, if the detected nanofibers are *C*−*S*−*H*, then another chemical reaction must have occurred to transform $Ca(OH)_2$ into different products. Alternatively, if the nanofibers are ettringite, their presence indirectly suggests that the primary hydration reactions are impeded with the introduction of biomatter even if cement has access to water to form the secondary reaction products. Finally, if the nanofibers are byproducts of biomatter and cement, this implies that biomatter would interfere with the primary hydration reaction of alite and belite, leading to the absence of both $Ca(OH)_2$ and *C*−*S*−*H*.

We conducted FTIR analyses to probe the potential chemical reactions between biomatter and cement (spectra presented in Figure 4f, main peak assignments listed in Table 2). The functional groups of chlorella include the predominant O−H bonds (stretching peak at 3600−3000 cm^{-1}), C═O and C−O bonds in COOH (C═O stretching peak at 1740−1730 cm^{-1}, C−O stretching peak at 1050−1020 cm^{-1}), and protein-related groups (amide I band at 1600−1700 cm^{-1} from C═O stretching and water O−H bending around 1640 cm^{-1}, amide II region from N−H bending and C−N stretching centered at 1540 cm^{-1}, and amide III vibrations of C−N stretching and N−H bending result in the weaker 1230−1240 cm^{-1} peaks).[44,60] In addition, we detect carbohydrate-related bands with multiple peaks (C−H stretching peak at 3000−2800 cm^{-1}, weak symmetric and asymmetric CH_3, CH_2, and C−H bending at 1375−1450 cm^{-1} from polysaccharides or lipids, C−O stretching peaks at 1075, 1095, and 1150 cm^{-1}, and C−C stretch from carbohydrates or alcohols at 1030 and 1050 cm^{-1}).[44,61]

Table 2. Characteristic FTIR Peaks of Chlorella and Hardened Portland Cement

	chlorella			pure cement	
	peak (cm^{-1})	bond type		peak (cm^{-1})	bond type
(a)	3000−3600	OH stretch	(h)	3643	OH stretch in $Ca(OH)_2$
(b)	2925	C−H stretch	(i)	3397	OH of H_2O in *C*−*S*−*H* or ettringite
(c)	1735	C═O stretch in COOH	(j)	1636	H_2O in ettringite and free water
(d)	1630−1650	C═O stretch in amide I, O−H stretch in H_2O	(k)	1411	CO_3 bending in $CaCO_3$
(e)	1540	N−H bend and C−N stretch in amide II	(l)	1111	SO_4 stretch in ettringite
(f)	1230−1240	C−N stretch, N−H bend in amide III	(m)	948	Si−O stretch in *C*−*S*−*H*
(g)	1023	C−O stretch in alcohols			

For pure cement (Figure 4f and Table 2), the sharp peak at 3640−3646 cm^{-1} corresponds to the OH stretching in $Ca(OH)_2$,[58,62,63] while the OH stretching in free water, *C*−*S*−*H*, or ettringite give rise to a broader peak centered at 3400 cm^{-1}.[63−65] The free water as well as the ettringite-bound water also results in an absorption band at 1640−1675 cm^{-1}.[63] The CO_3 out-of-plane bending in $CaCO_3$ is detected at 1400−1490 cm^{-1},[58,63] the SO_4 antisymmetrical stretching in ettringite at 1100−1120 cm^{-1},[63] and Si−O stretching in *C*−*S*−*H* at 950−980 cm^{-1}.[58,62,64]

Comparing the spectra of the chlorella composites with chlorella and pure cement (Figure 4f), we again find that the peak associated with $Ca(OH)_2$ (sharp OH stretching peak at ∼3640 cm^{-1}) is almost eliminated when chlorella content is higher than 5 wt %. Meanwhile, the peak at 1110 cm^{-1} for the SO_4 antisymmetrical stretching in ettringite appears consistently in all the composites. The broad peak between 3280 and 3400 cm^{-1} associated with the OH in H_2O in ettringite and *C*−*S*−*H* is found to be broader and more red-shifted with increasing chlorella content. In addition, the intensity of *C*−*S*−*H* associated with the Si−O peak at ∼948 cm^{-1} is significantly decreased at biomatter content higher than 5 wt % while the peak itself is also red-shifted. These findings imply that *C*−*S*−*H* is either absent or substantially altered in the composites with 5 wt % chlorella or higher. Together with the XRD data, which revealed a higher amount of alite and belite in those composites, our results suggest that the primary hydration reactions are hindered at biomatter content higher than 5 wt %.

To further investigate the micromorphology and composition of hydration products, we utilize EDS to identify the spatial distribution of elemental composition. In the hardened pure cement, we probe the morphologically distinct $Ca(OH)_2$ platelets (spots 1 and 2 in Figure 5a) which yield an O/Ca ratio of 2.9−3.6 as shown in Table 3. The value is reasonably higher than the stoichiometric 2 due to signal contributions from the neighboring matrix. Irregular reactant particles (spot 3 in Figure 5a) have a Ca/Si ratio of 1.8, close to the stoichiometric expectation of 2 for belite, while for alite, we anticipate a ratio of 3. Finally, targeting the *C*−*S*−*H* coating, which appears to have a flower-like fibrous form (spots 4−6 in Figure 5a), we measure a Ca/Si ratio of 1.6−2.6 (anticipated value 0.6−2.3[64,66]). Spot analysis of raw algal biomatter (Figure 5b) reveals carbon, nitrogen, and oxygen, as the top three elements found in that biomatter, which are present at

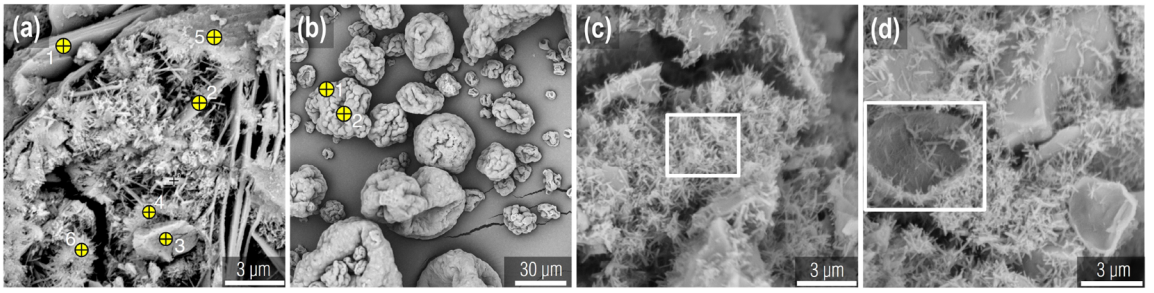

Figure 5. Composition profile of biocomposites. (a) Elemental ratio of hydration products in pure cement at day 28. (b) Composition profile of chlorella. (c) Composition profile of nanofibers and (d) spherical structures in the chlorella composite with 5 wt % biomatter.

https://doi.org/10.1021/acssuschemeng.2c07539
ACS Sustainable Chem. Eng. 2023, 11, 8242−8254

Table 3. Elemental Composition (Atomic Ratio) of Pure Cement, Raw Chlorella Powder, and the Nanofibers and Macrospheres of Composites with 5 wt % Chlorella

pure cement			raw chlorella			chlorella 5 wt %		
spot	products	*O/Ca* or Ca/Si	element	spot 1	spot 2	element	nanofibers	macrospheres
1	$Ca(OH)_2$	2.87	C	5.34	5.87	Ca	8.39	5.78
2	$Ca(OH)_2$	3.58	N	1.04	1.17	Si	1	1
3	Alite, Belite	1.84	O	1	1	N	1.58	3.52
4	*C−S−H*	2.6	P	0.04	0.21	O	4.57	18.14
5	*C−S−H*	1.62	S	0.02	0.17	S	1.29	1.20
6	*C−S−H*	2.34	Ca	0.02	0.07	Al	0.27	0.61

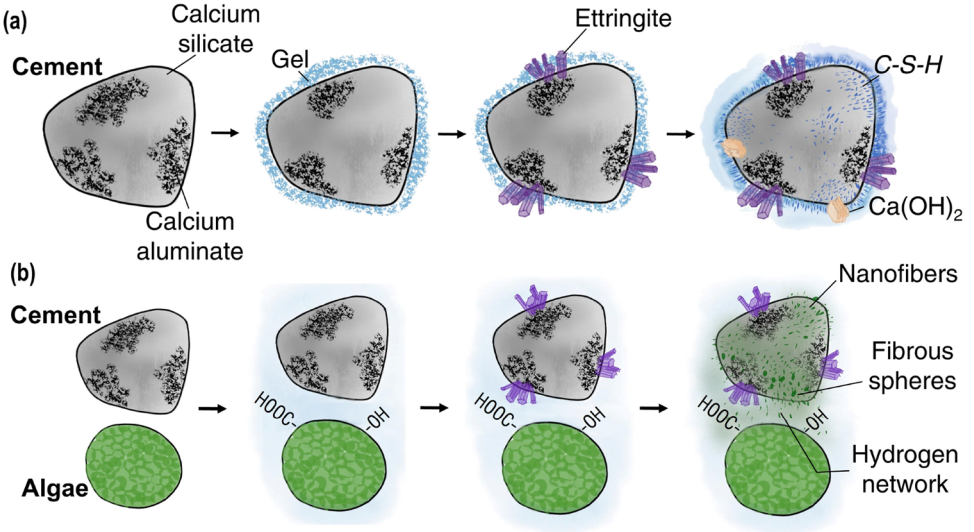

Figure 6. Hydration reactions of ordinary Portland cement and the altered hydration reaction with the addition of algal biomatter. (a) The hydration reaction of ordinary Portland cement. Upon contact with water, alite and belite form a gel surrounding the surface of cement. Ettringite generated from tricalcium aluminate precipitates in prisms. The primary hydration reaction of alite and belite starts, nucleating amorphous *C−S−H* fibrils and $Ca(OH)_2$ platelets. (b) The hydrophilic algal surfaces interact with cement particles in the presence of water. The secondary hydration reactions of cement still occur, creating ettringite precipitates. The acidified carboxylic and hydroxyl groups of the biomatter carbohydrates in alkaline conditions facilitate a strong hydrogen bond network which encapsulates cement particles, inhibiting the reaction of alite and belite, thereby hindering the formation of *C−S−H* and $Ca(OH)_2$ while forming nanofibers and microspheres of different compositions.

the ratio of 5.5:1.1:1 for chlorella and 2.3:0.87:1 for spirulina, reflecting the higher protein content of spirulina and higher carbohydrate content of chlorella.

Next, we focus on the two distinct micromorphological features of our composites revealed in the previous section, the nanofibers and spherical structures, seen in both the chlorella and spirulina composites, and acquire compositional maps (areas shown in Figure 5c,d). We observe that the nanofibers in both biocomposites show significantly higher Ca/Si ratio (4.5−9.0 for the 5 wt % chlorella and 3.1−5.2 for 5 wt % spirulina; see Table 3) than the ratio of 0.6−2.3 reported for *C−S−H* in pure cement,[64,66] so do the microspheres (5.5 and 8.6 for 5 wt % chlorella and spirulina, respectively). The measured high Ca/Si ratios confirm that the formed nanofibers are not *C−S−H*. Meanwhile, the presence of silica and low content of aluminum and sulfur corroborate that the nanofibers are not ettringite either, which is already suggested from the morphological analysis as it typically displays lengths in μm scale as shown in Figure 3b, unlike the consistent length of 500 nm we observed for the nanofibers. Interestingly, the nanofibers and spheres in both biocomposites show a notable N/Si ratio ranging from 1.6 to 4. Since there is no significant amount of nitrogen in pure cement, but there is in biomatter, the results suggest that the formed nanofibers and microspheres may be in fact new amorphous compounds derived from the distinct exothermic reaction between cement and algal biomatter observed in the IC results (Figure 4b) and associated with the new broad peaks found in the XRD patterns of spirulina composites.

Our results collectively suggest that the drastically different hydration behaviors and mechanical properties of the composites are dominated by chemical interactions between the functional groups on the biomatter surface and the inorganic cement colloid. The weakening mechanical performance of the biocomposites is the result of distinct hydration products instead of the structural defects alone. Chlorella and spirulina both have a high concentration of carbohydrates ranging from 13.6 to 54.4 wt % depending on strains and growth conditions, and for both, more than 50% of the carbohydrates have glucose monomers.[40,67−69] In alkaline conditions in cement pastes, glucose degrades into acidic forms such as parasaccharinic acid or glycolic acid, as demonstrated by Yang and Montgomery.[70] Therefore, we reasonably anticipate the acidification of glucose-based carbohydrates in both cases of chlorella and spirulina when mixed with the cement paste. Because of the alkaline and rich calcium cation (Ca^{2+}) environment, the new negatively charged end groups of the glucose-based carbohydrates would interact with the

https://doi.org/10.1021/acssuschemeng.2c07539
ACS Sustainable Chem. Eng. 2023, 11, 8242−8254

calcium cations, which can stabilize in chelated structures similar to calcium glycolate. Chaudhari et al.[71] demonstrated that both glycolic acid and calcium glycolate significantly delay the induction period in cement hydration reactions. In fact, they proposed that calcium glycolate adsorbs onto the alite surface, forming a stable hydrogen bond network. The hydrogen bond network then retards the diffusion of water to anhydrated cement, inhibiting the formation of hydration products ($Ca(OH)_2$ and $C-S-H$). This hypothesis is aligned with our observation that there is a concentration threshold above which the hydration retardation effect becomes a complete hindrance. At lower concentrations (<5 wt %), the hydration reactions of composites containing biomatter are delayed since the adsorption of calcium glycolate-like forms only partially cover the entire surface of anhydrated cement, inducing a prolonged diffusion process. However, at higher concentrations, when alite and belite are fully encapsulated by the screening hydrogen bond network of calcium glycolate-like carbohydrates, the hydration reactions are indefinitely delayed, thereby inhibiting the formation of $Ca(OH)_2$ and $C-S-H$. Similarly, Smith et al.[72] showed that the charged degradation forms of glucose nonselectively adsorb on ettringite through electrostatic interactions and, therefore, delay its secondary reaction with tricalcium aluminate that produces calcium aluminate monosulfate. However, they found that the reaction of tricalcium aluminate with gypsum and water to form ettringite is not blocked when the charged carbohydrates are present. This observation explains the consistent presence of ettringite in our composites, suggesting that the primary reaction that produces ettringite crystals is not hindered.

In summary, we propose a mechanism to explain the observed effects of polysaccharide-based compounds on the strength evolution of cement−algae biocomposites and propose a graphical summary in Figure 6. Upon water exposure, the secondary hydration reactions derived from tricalcium aluminate occur even in the presence of biomatter, generating ettringite precipitates. In both types of biomatter, acidified carbohydrates are formed in alkaline conditions, which upon calcium chelation and surface adsorption facilitate a strong hydrogen bond network ultimately encapsulating calcium silicates on the cement particles. The formed network inhibits the reaction of calcium silicates and water and, thus, hinders the formation of $C-S-H$ and $Ca(OH)_2$ while forming nanofibers and microspheres of different compositions. Moreover, the negative-charged carbohydrates adsorb on the positive-charged ettringite precipitates blocking their further reactions. The morphologically distinct microspheres and nanofibers, which are found to coat the reactant surfaces, are amorphous compounds with high amounts of nitrogen, suggesting protein-related products. We note that the presence of ettringite versus the absence of $Ca(OH)_2$ and $C-S-H$ in our composites could also be attributed to the different reaction rates of hydration reactions. As the tricalcium aluminate hydration happens faster, it is less influenced by the presence of biomatter, which interacts with both reactants and reaction products, while the slower hydration reactions of calcium silicates are affected more significantly. We have shown the hindrance effect induced by the algal biomatter is a chemical process, and therefore, more specific surface area (smaller particles) would likely exacerbate the hindrance effect.

Finally, to explain the different aging behavior between chlorella and spirulina and the higher strength evolution in spirulina composites, we note the different carbohydrate content in the two types of biomatter. We analyzed the carbohydrate content of our biomatters via high performance liquid chromatography (HPLC) (results shown in Figure S5 for chlorella and prior work from Fredricks et al.[40] for spirulina) and found that chlorella contains 21.7 wt % carbohydrates, 10.8 wt % of which are glucose-based, while spirulina has 14 wt % carbohydrates, 6.1 wt % of which are glucose-based. This result supports the more significant suppressing effect when chlorella is introduced in cement as compared to spirulina. A similar effect of wood flour in Portland cement at 7.5 wt % (wood flour/dry cement) was reported by Dong et al.[73] They showed that the wood with high content of sugar and sugar acid (poplar wood) inhibits the hydration process more than the Chinese fir (lower content of sugar and sugar acid). However, they reported that ettringite generation was not negatively affected by the presence of wood flour in either case, which agrees with our findings.

Potentials of Reducing Carbon Footprint. To provide insight into the potential of mitigating the carbon footprint using algal biomatter, we assess the environmental impact of our biocomposite cements through the quantification of specific CO_2 emissions as a function of algae concentration. Assuming that the algae is embedded in the cement paste and stored in the long term (will not decompose), the carbon-negative fillers can have beneficial environmental effects, for which we now provide an estimation. On one hand, the CO_2 emissions of anhydrated cement are commonly estimated to be 1 kg CO_2/kg anhydrated.[74] On the other hand, although the environmental impact of algae production is less straightforward to estimate as it strongly depends on culture conditions, the use of fertilizers, or harvesting and drying methods,[75−77] Liao et al.[78] estimated the overall (negative) carbon emission for microalgae to be approximately −0.54 kg CO_2 eq/kg of dry spirulina. Based on these values, the net reduction in specific CO_2 emissions of biocomposite cements compared to neat cements can be estimated as a function of filler concentration (see SI section Estimation of the Reduction of CO2 Emissions). As examples, we report values for algae concentrations of 0.5%, 1%, and 5% in Table 4. Such reductions in emissions could have beneficial effects on the environmental impact of cements.

Table 4. Variation in Strength and Specific CO_2 Emissions (kg CO_2/kg) for Biocomposite Cements Compared to Neat Cements

algae concentration (wt %)	specific CO_2 emissions reduction (%)
0.5	0.6
1	1.3
5	6.4

CONCLUSIONS

In this Article, we have investigated the effects of introducing spirulina and chlorella microalgae at different concentrations into Portland cement on the resulting mechanical properties, morphologies, and hydration kinetics via multiple characterization methods. Below 5 wt % algae concentration, the compressive strength evolution of the biocomposites and the onset of the primary hydration reaction are delayed. Adding more than 5 wt % of either algae, we find a drastic reduction in the long term compressive strength by 85% due to the

https://doi.org/10.1021/acssuschemeng.2c07539
ACS Sustainable Chem. Eng. 2023, 11, 8242−8254

hindrance effect of the primary hydration reactions, which leads to the absence of calcium hydroxide as quantified from the TGA, XRD, and FTIR results. For composites containing 5 wt % biomatter, we observed the appearance of a new exothermic reaction during the hardening process, which we correlated with the distinct morphologies and protein-related compositions of the nanofibers and spheres shown in the SEM and EDS. Focusing on the consistent presence of ettringite and the absence of $Ca(OH)_2$ and *C*−*S*−*H*, we proposed a mechanism to explain the concentration-dependent behavior of cement−algae composites based on the polysaccharide-based compounds. Including the carbon sequestration capacity of biomatter, our calculations suggest that 1.3% reduction of specific CO_2 is achievable with the addition of 1 wt % algal biomatter in Portland cement. Based on our fundamental analyses, we foresee future research in cements containing biomass with lower amounts of water-soluble carbohydrates, and we highlight the need to conduct molecular simulations to understand further the interactions between the components so that an improved performance can be achieved and further reductions of the environmental impact of cementitious materials can be realized.

■ ASSOCIATED CONTENT

Supporting Information

The Supporting Information is available free of charge at https://pubs.acs.org/doi/10.1021/acssuschemeng.2c07539.

> Measurement and theoretical estimation of apparent density; measurement of shrinkage; evaluation of the reduction of CO_2 emissions; compression tests and stress−strain curves of cement−spirulina composites; optical microscopy of the morphology and porosity of the cement−algae biocomposites; SEM snapshots of cement−spirulina composites; shrinkage of cement−chlorella and cement−spirulina composites; the apparent density of cement−algae biocomposites at different concentrations; pore water quantification in pure cement, cement−spirulina, and cement−chlorella composites; XRD patterns and phase evolution of cement−spirulina composites; carbohydrate content measurements in chlorella (PDF)

■ AUTHOR INFORMATION

Corresponding Author

Eleftheria Roumeli − *Department of Materials Science and Engineering, University of Washington, Seattle, Washington 98195, United States;* orcid.org/0000-0002-2828-1428; Email: eroumeli@uw.edu

Authors

Meng-Yen Lin − *Department of Materials Science and Engineering, University of Washington, Seattle, Washington 98195, United States*

Paul Grandgeorge − *Department of Materials Science and Engineering, University of Washington, Seattle, Washington 98195, United States*

Andrew M. Jimenez − *Department of Materials Science and Engineering, University of Washington, Seattle, Washington 98195, United States;* orcid.org/0000-0001-7696-9705

Bichlien H. Nguyen − *Microsoft Research, Redmond, Washington 98052-5321, United States; Paul G. Allen School of Computer Science and Engineering, University of Washington, Seattle, Washington 98195, United States*

Complete contact information is available at: https://pubs.acs.org/10.1021/acssuschemeng.2c07539

Notes

The authors declare no competing financial interest.

■ ACKNOWLEDGMENTS

The authors thank Brandon Lou, Li-Yuan Lin, and Konstantina Mason for assisting in the preliminary biocomposite sample fabrication and mechanical testing. The authors thank Prof. Renata Bura and Jeffrey Hsu for the HPLC tests and Michael Mathews and Viviana Costa from TA Instruments for the IC tests. Part of the characterizations were performed at the Washington Clean Energy Testbeds (WCET). The authors acknowledge financial support in the form of gift funds from Microsoft Research.

■ REFERENCES

(1) Adams, M.; Burrows, V.; Richardson, S.; Drinkwater, J.; Gamboa, C.; Collin, C.; Den, X.; Riemann, L.; Porteron, S.; Secher, A. *Bringing embodied carbon upfront: Coordinated action for the building and construction sector to tackle embodied carbon*; 2019; https://www.worldgbc.org/embodied-carbon.

(2) Worrell, E.; Price, L.; Martin, N.; Hendriks, C.; Meida, L. O. Carbon Dioxide Emissions from the Global Cement Industry. *Annual Review of Energy and the Environment* **2001**, *26*, 303−329.

(3) Humphreys, K.; Mahasenan, M. *Towards a sustainable cement industry. Substudy 8: climate change*; 2002; https://www.osti.gov/etdeweb/biblio/20269589.

(4) Palkovic, S. D.; Brommer, D. B.; Kupwade-Patil, K.; Masic, A.; Buehler, M. J.; Büyüköztürk, O. Roadmap across the mesoscale for durable and sustainable cement paste − A bioinspired approach. *Construction and Building Materials* **2016**, *115*, 13−31.

(5) Duque-Redondo, E.; Masoero, E.; Manzano, H. Nanoscale shear cohesion between cement hydrates: The role of water diffusivity under structural and electrostatic confinement. *Cem. Concr. Res.* **2022**, *154*, 106716.

(6) Zhou, T.; Ioannidou, K.; Ulm, F.-J.; Bazant, M. Z.; Pellenq, R. J.-M. Multiscale poromechanics of wet cement paste. *Proc. Natl. Acad. Sci. U. S. A.* **2019**, *116*, 10652−10657.

(7) Ioannidou, K.; Krakowiak, K. J.; Bauchy, M.; Hoover, C. G.; Masoero, E.; Yip, S.; Ulm, F.-J.; Levitz, P.; Pellenq, R. J.-M.; Del Gado, E. Mesoscale texture of cement hydrates. *Proc. Natl. Acad. Sci. U. S. A.* **2016**, *113*, 2029−2034.

(8) Hendriks, C. A.; Worrell, E.; De Jager, D.; Blok, K.; Riemer, P. Emission reduction of greenhouse gases from the cement industry. *Proceedings of the fourth international conference on greenhouse gas control technologies* **1999**, 939−944.

(9) Arehart, J. H.; Nelson, W. S.; Srubar III, W. V. On the theoretical carbon storage and carbon sequestration potential of hempcrete. *Journal of Cleaner Production* **2020**, *266*, 121846.

(10) Chousidis, N.; Rakanta, E.; Ioannou, I.; Batis, G. Mechanical properties and durability performance of reinforced concrete containing fly ash. *Construction and Building Materials* **2015**, *101*, 810−817.

(11) Islam, G. S.; Rahman, M.; Kazi, N. Waste glass powder as partial replacement of cement for sustainable concrete practice. *International Journal of Sustainable Built Environment* **2017**, *6*, 37−44.

(12) Cordeiro, G.; Toledo Filho, R.; Tavares, L.; Fairbairn, E. Experimental characterization of binary and ternary blended-cement concretes containing ultrafine residual rice husk and sugar cane bagasse ashes. *Construction and Building Materials* **2012**, *29*, 641−646.

(13) Vijay, K.; Murmu, M.; Deo, S. V. Bacteria based self healing concrete—A review. *Construction and Building Materials* **2017**, *152*, 1008—1014.
(14) Menon, R. R.; Luo, J.; Chen, X.; Zhou, H.; Liu, Z.; Zhou, G.; Zhang, N.; Jin, C. Screening of fungi for potential application of self-healing concrete. *Sci. Rep.* **2019**, *9*, 1—12.
(15) Nguyen, P. Q.; Courchesne, N.-M. D.; Duraj-Thatte, A.; Praveschotinunt, P.; Joshi, N. S. Engineered Living Materials: Prospects and Challenges for Using Biological Systems to Direct the Assembly of Smart Materials. *Adv. Mater.* **2018**, *30*, 1704847.
(16) De Belie, N.; Gruyaert, E.; Al-Tabbaa, A.; Antonaci, P.; Baera, C.; Bajare, D.; Darquennes, A.; Davies, R.; Ferrara, L.; Jefferson, T.; et al. A review of self-healing concrete for damage management of structures. *Advanced materials interfaces* **2018**, *5*, 1800074.
(17) Wang, S.; Scarlata, S. F.; Rahbar, N. A self-healing enzymatic construction material. *Matter* **2022**, *5*, 957—974.
(18) Onuaguluchi, O.; Panesar, D. K.; Sain, M. Properties of nanofibre reinforced cement composites. *Construction and Building Materials* **2014**, *63*, 119—124.
(19) Cao, Y.; Zavaterri, P.; Youngblood, J.; Moon, R.; Weiss, J. The influence of cellulose nanocrystal additions on the performance of cement paste. *Cement and Concrete Composites* **2015**, *56*, 73—83.
(20) Barnat-Hunek, D.; Szymańska-Chargot, M.; Jarosz-Hadam, M.; Łagód, G. Effect of cellulose nanofibrils and nanocrystals on physical properties of concrete. *Construction and Building Materials* **2019**, *223*, 1—11.
(21) Guo, A.; Sun, Z.; Sathitsuksanoh, N.; Feng, H. A Review on the Application of Nanocellulose in Cementitious Materials. *Nanomaterials* **2020**, *10*, 2476.
(22) Fu, T.; Moon, R. J.; Zavattieri, P.; Youngblood, J.; Weiss, W. J. *Cellulose-Reinforced Nanofibre Composites*; Elsevier, 2017; pp 455—482; DOI: 10.1016/b978-0-08-100957-4.00020-6.
(23) Fu, T.; Montes, F.; Suraneni, P.; Youngblood, J.; Weiss, J. The Influence of Cellulose Nanocrystals on the Hydration and Flexural Strength of Portland Cement Pastes. *Polymers* **2017**, *9*, 424.
(24) Laborel-Préneron, A.; Aubert, J. E.; Magniont, C.; Tribout, C.; Bertron, A. Plant aggregates and fibers in earth construction materials: A review. *Construction and Building Materials* **2016**, *111*, 719—734.
(25) Akinyemi, A. B.; Omoniyi, E. T.; Onuzulike, G. Effect of microwave assisted alkali pretreatment and other pretreatment methods on some properties of bamboo fibre reinforced cement composites. *Construction and Building Materials* **2020**, *245*, 118405.
(26) Ban, Y.; Zhi, W.; Fei, M.; Liu, W.; Yu, D.; Fu, T.; Qiu, R. Preparation and Performance of Cement Mortar Reinforced by Modified Bamboo Fibers. *Polymers* **2020**, *12*, 2650.
(27) Bilba, K.; Arsene, M.-A.; Ouensanga, A. Sugar cane bagasse fibre reinforced cement composites. Part I. Influence of the botanical components of bagasse on the setting of bagasse/cement composite. *Cement and Concrete Composites* **2003**, *25*, 91—96.
(28) Rahimi, M.; Hisseine, O. A.; Tagnit-Hamou, A. Effectiveness of treated flax fibers in improving the early age behavior of high-performance concrete. *Journal of Building Engineering* **2022**, *45*, 103448.
(29) Ahmad, M. R.; Chen, B. Influence of type of binder and size of plant aggregate on the hygrothermal properties of bio-concrete. *Construction and Building Materials* **2020**, *251*, 118981.
(30) Zeller, M. A.; Hunt, R.; Jones, A.; Sharma, S. Bioplastics and their thermoplastic blends from Spirulina and Chlorella microalgae. *J. Appl. Polym. Sci.* **2013**, *130*, 3263—3275.
(31) Gavrilescu, M.; Chisti, Y. Biotechnology—a sustainable alternative for chemical industry. *Biotechnology advances* **2005**, *23*, 471—499.
(32) Mirón, A. S.; Garcıa, M. C. C.; Gómez, A. C.; Camacho, F. G.; Grima, E. M.; Chisti, Y. Shear stress tolerance and biochemical characterization of Phaeodactylum tricornutum in quasi steady-state continuous culture in outdoor photobioreactors. *Biochemical Engineering Journal* **2003**, *16*, 287—297.
(33) Chisti, Y. Biodiesel from microalgae. *Biotechnology advances* **2007**, *25*, 294—306.
(34) León-Martínez, F.; Cano-Barrita, P. d. J.; Lagunez-Rivera, L.; Medina-Torres, L. Study of nopal mucilage and marine brown algae extract as viscosity-enhancing admixtures for cement based materials. *Construction and Building Materials* **2014**, *53*, 190—202.
(35) Hernández, E.; Cano-Barrita, P. d. J.; Torres-Acosta, A. Influence of cactus mucilage and marine brown algae extract on the compressive strength and durability of concrete. *Materiales de Construcción* **2016**, *66*, e074—e074.
(36) Aday, A. N.; Osio-Norgaard, J.; Foster, K. E.; Srubar, W. V. Carrageenan-based superabsorbent biopolymers mitigate autogenous shrinkage in ordinary portland cement. *Materials and Structures* **2018**, *51*, 1—13.
(37) Clarkson, C. M.; El Awad Azrak, S. M.; Forti, E. S.; Schueneman, G. T.; Moon, R. J.; Youngblood, J. P. Recent developments in cellulose nanomaterial composites. *Adv. Mater.* **2021**, *33*, 2000718.
(38) McHugh, D. J. *Production and utilization of products from commercial seaweeds*; FAO, 1987; ISBN: 92-5-102612-2.
(39) Manuhara, G. J.; Praseptiangga, D.; Riyanto, R. A. Extraction and characterization of refined K-carrageenan of red algae [Kappaphycus Alvarezii (Doty ex PC Silva, 1996)] originated from Karimun Jawa Islands. *Aquatic Procedia* **2016**, *7*, 106—111.
(40) Fredricks, J. L.; Iyer, H.; McDonald, R.; Hsu, J.; Jimenez, A. M.; Roumeli, E. Spirulina-based composites for 3D-printing. *J. Polym. Sci.* **2021**, *59*, 2878—2894.
(41) Roumeli, E.; Hendrickx, R.; Bonanomi, L.; Vashisth, A.; Rinaldi, K.; Daraio, C. Biological matrix composites from cultured plant cells. *Proc. Natl. Acad. Sci. U. S. A.* **2022**, *119*, e2119523119.
(42) Duraj-Thatte, A. M.; Manjula-Basavanna, A.; Courchesne, N.-M. D.; Cannici, G. I.; Sánchez-Ferrer, A.; Frank, B. P.; van't Hag, L.; Cotts, S. K.; Fairbrother, D. H.; Mezzenga, R.; et al. Water-processable, biodegradable and coatable aquaplastic from engineered biofilms. *Nat. Chem. Biol.* **2021**, *17*, 732—738.
(43) Campbell, I.; Lin, M.-Y.; Iyer, H.; Parker, M.; Fredricks, J.; Liao, K.; Jimenez, A.; Grandgeorge, P.; Roumeli, E. Progress in Sustainable Polymers from Biological Matter. *Annu. Rev. Mater. Res.* **2023**, *53*, 1.
(44) Chen, X.; Matar, M. G.; Beatty, D. N.; Srubar, W. V. Retardation of Portland Cement Hydration with Photosynthetic Algal Biomass. *ACS Sustainable Chem. Eng.* **2021**, *9*, 13726—13734.
(45) ASTM International. *Standard Specification for Portland Cement*; ASTM International, 2021.
(46) ASTM International. *Standard Test Method for Compressive Strength of Hydraulic Cement Mortars (Using 2-in. or [50 mm] Cube Specimens)*; ASTM International, 2021.
(47) Schneider, C. A.; Rasband, W. S.; Eliceiri, K. W. NIH Image to ImageJ: 25 years of image analysis. *Nat. Methods* **2012**, *9*, 671—675.
(48) Mehta, P. Scanning electron micrographic studies of ettringite formation. *Cem. Concr. Res.* **1976**, *6*, 169—182.
(49) Luo, S.; Liu, M.; Yang, L.; Chang, J. Effects of drying techniques on the crystal structure and morphology of ettringite. *Construction and Building Materials* **2019**, *195*, 305—311.
(50) Jennings, H.; Dalgleish, B.; Pratt, P. Morphological development of hydrating tricalcium silicate as examined by electron microscopy techniques. *J. Am. Ceram. Soc.* **1981**, *64*, 567—572.
(51) Pane, I.; Hansen, W. Investigation of blended cement hydration by isothermal calorimetry and thermal analysis. *Cement and Concrete Research* **2005**, *35*, 1155—1164.
(52) Rupasinghe, M.; San Nicolas, R.; Mendis, P.; Sofi, M.; Ngo, T. Investigation of strength and hydration characteristics in nano-silica incorporated cement paste. *Cement and Concrete Composites* **2017**, *80*, 17—30.
(53) Jiang, C.; Yu, L.; Tang, X.; Chu, H.; Jiang, L. Deterioration process of high belite cement paste exposed to sulfate attack, calcium leaching and the dual actions. *Journal of Materials Research and Technology* **2021**, *15*, 2982—2992.
(54) Linggawati, A. Preparation and characterization of calcium oxide heterogeneous catalyst derived from Anadara granosa shell for biodiesel synthesis. *KnE Engineering* **2016**, *1*, 1—8.

(55) Kontoleontos, F.; Tsakiridis, P.; Marinos, A.; Katsiotis, N.; Kaloidas, V.; Katsioti, M. Dry-grinded ultrafine cements hydration. physicochemical and microstructural characterization. *Mater. Res.* **2013**, *16*, 404−416.
(56) Jadhav, R.; Debnath, N. Computation of X-ray powder diffractograms of cement components and its application to phase analysis and hydration performance of OPC cement. *Bulletin of Materials Science* **2011**, *34*, 1137−1150.
(57) Monteagudo, S.; Moragues, A.; Gálvez, J.; Casati, M.; Reyes, E. The degree of hydration assessment of blended cement pastes by differential thermal and thermogravimetric analysis. Morphological evolution of the solid phases. *Thermochim. Acta* **2014**, *592*, 37−51.
(58) Flores, J.; Kamali, M.; Ghahremaninezhad, A. An investigation into the properties and microstructure of cement mixtures modified with cellulose nanocrystal. *Materials* **2017**, *10*, 498.
(59) Baston, G.; Clacher, A.; Heath, T.; Hunter, F.; Smith, V.; Swanton, S. Calcium silicate hydrate (CSH) gel dissolution and pH buffering in a cementitious near field. *Mineralogical Magazine* **2012**, *76*, 3045−3053.
(60) Barón-Sola, Á.; Toledo-Basantes, M.; Arana-Gandía, M.; Martínez, F.; Ortega-Villasante, C.; Dučić, T.; Yousef, I.; Hernández, L. E. Synchrotron Radiation-Fourier Transformed Infrared microspectroscopy (μSR-FTIR) reveals multiple metabolism alterations in microalgae induced by cadmium and mercury. *J. Hazard. Mater.* **2021**, *419*, 126502.
(61) Šimonovičová, A.; Takáčová, A.; Šimkovic, I.; Nosalj, S. Experimental treatment of hazardous ash waste by microbial consortium Aspergillus niger and Chlorella sp.: decrease of the Ni content and identification of adsorption sites by FTIR spectroscopy. *Frontiers in Microbiology* **2021**, *12*, 3820.
(62) Li, G. Y.; Wang, P. M.; Zhao, X. Mechanical behavior and microstructure of cement composites incorporating surface-treated multi-walled carbon nanotubes. *Carbon* **2005**, *43*, 1239.
(63) Fernández-Carrasco, L.; Torrens-Martín, D.; Morales, L.; Martínez-Ramírez, S. Infrared spectroscopy in the analysis of building and construction materials. In *Infrared spectroscopy−Materials science, engineering and technology*; IntechOpen, 2012; DOI: 10.5772/36186.
(64) Pelisser, F.; Gleize, P. J. P.; Mikowski, A. Effect of the Ca/Si molar ratio on the micro/nanomechanical properties of synthetic CSH measured by nanoindentation. *J. Phys. Chem. C* **2012**, *116*, 17219−17227.
(65) Gastaldi, D.; Canonico, F.; Boccaleri, E. Ettringite and calcium sulfoaluminate cement: investigation of water content by near-infrared spectroscopy. *J. Mater. Sci.* **2009**, *44*, 5788−5794.
(66) Zhang, Z.; Scherer, G.; Bauer, A. Morphology of cementitious material during early hydration. *Cem. Concr. Res.* **2018**, *107*, 85.
(67) Safi, C.; Zebib, B.; Merah, O.; Pontalier, P.-Y.; Vaca-Garcia, C. Morphology, composition, production, processing and applications of Chlorella vulgaris: A review. *Renewable and Sustainable Energy Reviews* **2014**, *35*, 265−278.
(68) El-Naggar, N. E.-A.; Hussein, M. H.; Shaaban-Dessuuki, S. A.; Dalal, S. R. Production, extraction and characterization of Chlorella vulgaris soluble polysaccharides and their applications in AgNPs biosynthesis and biostimulation of plant growth. *Sci. Rep.* **2020**, *10*, 1−19.
(69) Shekharam, K. M.; Venkataraman, L.; Salimath, P. Carbohydrate composition and characterization of two unusual sugars from the blue green alga Spirulina platensis. *Phytochemistry* **1987**, *26*, 2267−2269.
(70) Yang, B. Y.; Montgomery, R. Alkaline degradation of glucose: effect of initial concentration of reactants. *Carbohydrate research* **1996**, *280*, 27−45.
(71) Chaudhari, O.; Biernacki, J. J.; Northrup, S. Effect of carboxylic and hydroxycarboxylic acids on cement hydration: experimental and molecular modeling study. *J. Mater. Sci.* **2017**, *52*, 13719−13735.
(72) Smith, B. J.; Rawal, A.; Funkhouser, G. P.; Roberts, L. R.; Gupta, V.; Israelachvili, J. N.; Chmelka, B. F. Origins of saccharide-dependent hydration at aluminate, silicate, and aluminosilicate surfaces. *Proc. Natl. Acad. Sci. U. S. A.* **2011**, *108*, 8949−8954.
(73) Dong, Z.; Yu, Y.; Song, P.; Ma, L.; Lu, F. Effects of Two Types of Waste Wood Species on the Hydration Characteristic of Portland Cement. *Journal of Advanced Concrete Technology* **2016**, *14*, 13−20.
(74) Ali, M. B.; Saidur, R.; Hossain, M. S. A review on emission analysis in cement industries. *Renewable and Sustainable Energy Reviews* **2011**, *15*, 2252−2261.
(75) Tzachor, A.; Smidt-Jensen, A.; Ramel, A.; Geirsdóttir, M. Environmental impacts of large-scale Spirulina (Arthrospira platensis) production in Hellisheidi geothermal park Iceland: life cycle assessment. *Marine Biotechnology* **2022**, *24*, 991−1001.
(76) Beckstrom, B. D.; Wilson, M. H.; Crocker, M.; Quinn, J. C. Bioplastic feedstock production from microalgae with fuel co-products: A techno-economic and life cycle impact assessment. *Algal Research* **2020**, *46*, 101769.
(77) Ye, C.; Mu, D.; Horowitz, N.; Xue, Z.; Chen, J.; Xue, M.; Zhou, Y.; Klutts, M.; Zhou, W. Life cycle assessment of industrial scale production of spirulina tablets. *Algal Research* **2018**, *34*, 154−163.
(78) Liao, K.; Grandgeorge, P.; Jimenez, A. M.; Nguyen, B. H.; Roumeli, E. Effects of mechanical cell disruption on the morphology and properties of spirulina-PLA biocomposites. *Sustainable Materials and Technologies* **2023**, *36*, e00591.